High-Quality, Highly Concentrated Semiconducting Single-Wall Carbon Nanotubes for Use in Field Effect Transistors and Biosensors

Wen-Shan Li,[†] Peng-Xiang Hou,[†] Chang Liu,[*] Dong-Ming Sun, Jiangtan Yuan, Shi-Yong Zhao, Li-Chang Yin, Hongtao Cong, and Hui-Ming Cheng

Shenyang National Laboratory for Materials Science, Institute of Metal Research, Chinese Academy of Sciences, Shenyang 110016, People's Republic of China. [†]These authors contributed equally to this work.

ABSTRACT We developed a simple and scalable selective synthesis method of high-quality, highly concentrated semiconducting single-wall carbon nanotubes (s-SWCNTs) by *in situ* hydrogen etching. Samples containing ~93% s-SWCNTs were obtained in bulk. These s-SWCNTs with good structural integrity showed a high oxidation resistance temperature of ~800 °C. Thin-film transistors based on the s-SWCNTs demonstrated a high carrier mobility of 21.1 $cm^2 V^{-1} s^{-1}$ at an on/off ratio of 1.1×10^4 and a high on/off ratio of 4.0×10^5 with a carrier mobility of 7.0 $cm^2 V^{-1} s^{-1}$. A biosensor fabricated using the s-SWCNTs had a very low dopamine detection limit of 10^{-18} mol/L at room temperature.

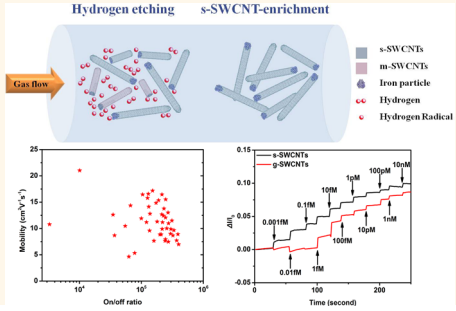

KEYWORDS: carbon nanotube · CVD · semiconducting · thin-film transistor · sensor

Single-wall carbon nanotubes (SWCNTs) can be either semiconducting or metallic, depending on their chiralities. This feature enables SWCNTs to have potential use in high-performance nanodevices, such as field effect transistors (FETs), sensors, and ballistically conductive interconnects.[1,2] Each of these applications, however, requires a pure and high-quality SWCNT sample that contains only semiconducting or metallic nanotubes. Recently, notable progress has been made on the preparation of SWCNTs with controlled transport properties. This is basically achieved in two ways. One is by postsynthesis treatment including ultracentrifugation, electrophoresis, chromatography, selective solubilization, *etc.*[3−10] The drawback of this approach is that contaminations and defects are inevitably introduced during the dispersion and separation of the SWCNTs, and the nanotubes obtained are usually shortened to a submicrometer length. The other approach is to obtain semiconducting SWCNTs (s-SWCNTs) by *in situ* or postsynthesis selective etching, which is based on the principle that metallic SWCNTs (m-SWCNTs) are more chemically active than s-SWCNTs and would be preferentially removed under appropriate conditions. For example, an ethanol/methanol mixture,[11] oxygen gas,[12] water vapor,[13] and metal oxide[14] have been used as oxidative etchants to selectively remove m-SWCNTs. Although these oxidants have proved effective in etching m-SWCNTs, some disadvantages are also observed. For instance, some s-SWCNTs are removed at the same time, and the yield of s-SWCNTs is usually very limited; more importantly, the remaining s-SWCNTs usually contain many defects and have a shortened length, leading to poor oxidation resistance and low carrier mobility when serving as the channel material of FETs.[12] This is because carbon tends to strongly react with these oxidants at high temperatures, and it is very difficult to precisely control the selective removal of m-SWCNTs without damaging s-SWCNTs. It is therefore important and desirable to develop a milder selective etching method for the bulk preparation of s-SWCNTs with good structural integrity and high concentration.

* Address correspondence to cliu@imr.ac.cn.

Received for review April 22, 2013 and accepted July 22, 2013.

Published online July 22, 2013
10.1021/nn401998r

Hydrogen is a commonly used carrier gas for the synthesis of SWCNTs. It is usually considered to be unreactive with SWCNTs, although atomic hydrogen produced in methane or hydrogen plasma has been reported to be able to etch carbon nanotubes (CNTs).[15−17] When synthesizing SWCNTs by arc discharge using hydrogen as a buffer gas, we found that the amount of amorphous carbon impurity in the product was significantly decreased.[18,19] This means that molecular hydrogen can decompose and react with carbonaceous materials at high temperatures (*e.g.*, ~4000 K). In addition, hydrogen was found to dissociate at very low temperatures in the presence of Fe nanoparticles,[20,21] and as a result, SWCNTs with diameters smaller than 1.2 nm were preferentially eliminated. In addition, m-SWCNTs have been shown to be more reactive than s-SWCNTs with a similar diameter because of their relatively smaller ionization potential.[22] Therefore, it seems possible to remove m-SWCNTs by *in situ* hydrogen etching. Because hydrogen is a much milder etchant than previously reported oxidants, the SWCNTs obtained would possess better structural integrity and satisfy the demands of many applications.

In this work, we prepared high-quality s-SWCNTs in a high concentration by *in situ* selective removal of m-SWCNTs by hydrogen etching during a floating catalyst chemical vapor deposition (FCCVD) process. As a result, samples containing more than 90% s-SWCNTs were reproducibly obtained. The s-SWCNTs exhibit oxidation resistance in air up to 800 °C. Thin-film transistors (TFTs) using the s-SWCNTs as a channel material showed a high on/off ratio up to 4.0×10^5 (with a carrier mobility of 7.0 $cm^2\ V^{-1}\ s^{-1}$) and a high carrier mobility of 21.1 $cm^2\ V^{-1}\ s^{-1}$ (with an on/off ratio of 1.1×10^4). Biosensors fabricated using these s-SWCNTs demonstrated an ultralow detection limit (10^{-18} mol/L in a phosphate-buffered saline (PBS) solution) for dopamine detection.

RESULTS AND DISCUSSION

SWCNTs were prepared by FCCVD[12] using methane as carbon source, ferrocene as catalyst precursor, sulfur as growth promoter, and hydrogen as both carrier gas and etchant. A schematic of the synthesis, collection, and device fabrication process of s-SWCNTs is shown in Supporting Information Figure S1. Systematic experiments were performed to optimize the *in situ* hydrogen etching conditions to obtain a high concentration of s-SWCNTs, and the flux of hydrogen was found to be a critical parameter. We fixed the following growth parameters: temperature 1100 °C, CH_4 flow 30 sccm, catalyst precursor sublimation temperature 85 °C, and the hydrogen flows of 500, 1000, 2000, 3000, and 4000 sccm. The SWCNT samples obtained with these different hydrogen fluxes are denoted 1#, 2#, 3#, 4#, and 5#, respectively. These samples were examined by Raman spectroscopy with excitation laser wavelengths of 532, 633, and 785 nm. Figure 1a−c shows typical radial breathing mode (RBM) peaks of the above samples, where the peaks originating from m- and s-SWCNTs are highlighted according to the Kataura plot.[23−25] When a relatively low hydrogen flow was used, RBM peaks from both m- and s-SWCNTs were detected, indicating that the product is a mixture of m- and s-SWCNTs. When the hydrogen flow was increased to 2000 sccm, the m-SWCNT signal becomes undetectable in sample 3# for all three excitation laser wavelengths. A similar result is obtained from their typical G bands excited by the 633 nm laser, as shown in Figure 1d. It can be seen that the G^- band of samples 1#, 2#, 4#, and 5# exhibits the apparent characteristic of asymmetric Breit−Wigner−Fano (BWF) line shapes,[26,27] while that of sample 3# shows a different line shape. An obvious peak appearing at about 1570 cm^{-1} for sample 3# is identified as the G^- band from s-SWCNTs,[15] and a slight upshift of the G^+ mode is also a typical sign of a s-SWCNT-enriched sample.[28] These results indicate that sample 3# is rich in s-SWCNTs. In addition, sample 3# also has the highest I_G/I_D value (81.3) among the five samples (after intensity normalization of the G mode), suggesting better graphitic layer stacking. When the hydrogen flow was further increased to 3000 and 4000 sccm, the RBM peaks of both m-SWCNTs and s-SWCNTs were observed again. Therefore, the optimum hydrogen flow is determined to be 2000 sccm for the current growth temperature and catalyst concentration. A good reproducibility of the synthesis of enriched s-SWCNTs was further verified by multiwavelength laser Raman measurements of multibatch samples (3#) (see Figure S2).

Figure 2a,b shows representative scanning electron microscope (SEM) and transmission electron microscope (TEM) images of the prepared s-SWCNTs (sample 3#). The SEM image shows that the nanotubes are pure and form a random network. High-resolution TEM (HRTEM) observations reveal the uniform diameter and very straight carbon layer of the SWCNTs. It is worth noting that the amount of amorphous carbon is very small in the as-prepared SWCNT sample. The diameters of 150 SWCNTs were measured under TEM, and a histogram of the diameter distribution is plotted in Figure 2c. The diameters are distributed in the range of 1.5−2.5 nm and largely centered at 1.7−2.0 nm (~69%). The sample was purified by air oxidation at 350 °C and washing in hydrochloric acid (HCl solution) to remove residual catalyst and amorphous carbon prior to thermogravimetric (TG) analysis in air[29] to verify the structural integrity of the SWCNTs. Figure 2d shows that rapid oxidation does not occur until a temperature as high as 800 °C, approaching that for graphitized MWCNTs (~800 °C) and double-wall CNTs produced by arc-discharge (802 °C).[30,31] To the best of our knowledge, this is the highest oxidation

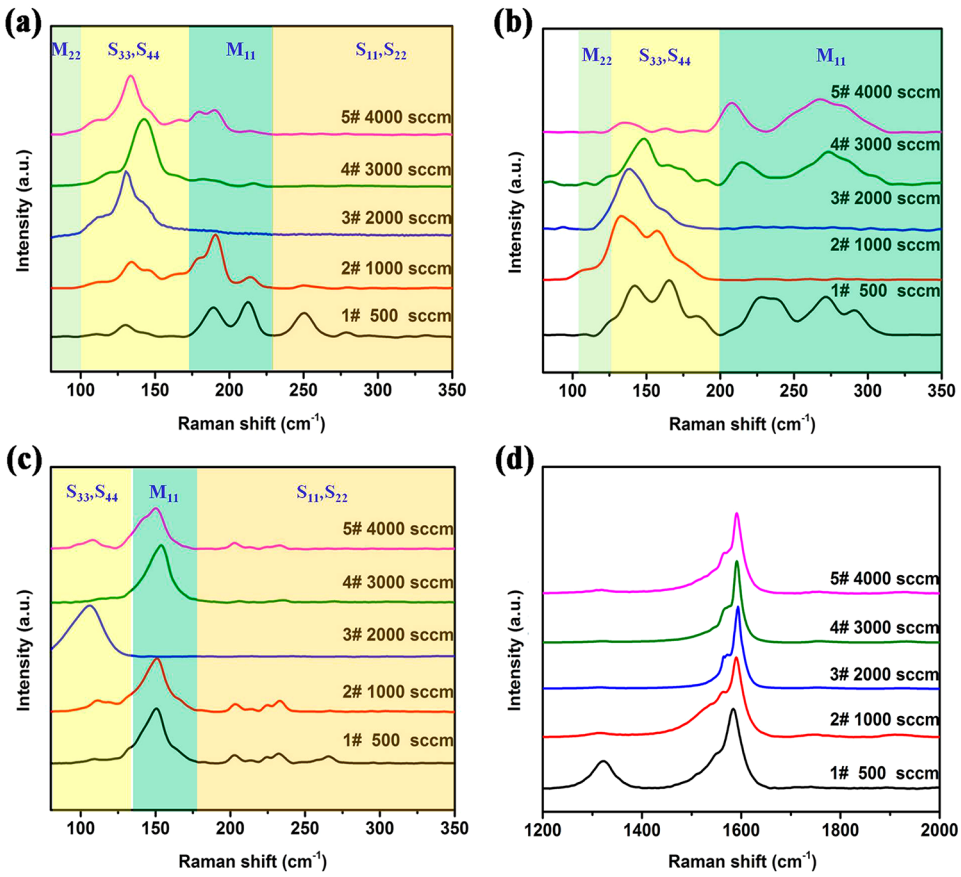

Figure 1. Laser Raman spectra of the as-prepared SWCNT samples. Typical RBM peaks of the SWCNTs obtained using hydrogen flows of 500, 1000, 2000, 3000, and 4000 sccm (denoted 1#−5#) with excitation laser wavelengths of (a) 633 nm, (b) 532 nm, and (c) 785 nm. (d) D band and G band of the SWCNT samples with the excitation laser wavelength of 633 nm.

resistance temperature reported for SWCNTs, indicating the perfect graphitic wall structure of the SWCNTs. Furthermore, the derivative thermogravimetric analysis (DTG) curve shows only one sharp peak narrowly distributed in the range of 620−850 °C, suggesting the high purity and uniform structure of the s-SWCNTs, which is consistent with the results from Raman, SEM, and TEM characterizations.

Optical absorption spectra of these samples were measured to further confirm the enrichment of s-SWCNTs and to estimate their content quantitatively. Typical UV−vis−NIR spectra are shown in Figure 3a. The spectroscopic characterization was performed using as-prepared SWCNT thin films collected from the downstream of the reactor using a mixed cellulose ester membrane (MCEM) (for details, see Figure S1 and S1.3). For sample 3#, two broad absorption bands located at 0.78−1.38 and 0.50−0.78 eV are clearly observed, which correspond to the first and second van Hove singularity transition of small s-SWCNT bundles (S_{11}, S_{22}). In contrast, no peak originating from the first van Hove singularity transition of m-SWCNTs (M_{11}) in the range of 1.38−2.49 eV can be observed.[25] This result further verifies that the 3# sample is composed of mostly s-SWCNTs. To estimate the relative weight ratio of metallic-to-semiconducting nanotubes in the samples, the background of the spectra was subtracted based on the nonlinear model (the detailed calculations are described in S2),[32−34] and the resulting s-SWCNT contents are marked in Figure 3b. The weight ratios (r) of metallic tubes (W_M) to semiconducting tubes (W_S) were estimated from the corresponding absorption peak areas using the formula $r = W_M/(W_S + W_M)$. The r value for sample 1# is 34.3%, which means that there is almost no m- and s-SWCNT selectivity when a small amount of hydrogen is used, agreeing with the previously reported results.[35] The smallest r value of 0.07 was achieved for sample 3#, confirming that m-SWCNTs can be effectively removed by introducing an optimum amount of hydrogen. The s-SWCNT content of sample 3# is estimated to be ~93.0%.

The above results suggest that high-quality, highly concentrated s-SWCNTs are prepared when an optimum amount of hydrogen is introduced in the FCCVD production process, which can be attributed to the selective hydrogen etching of m-SWCNTs. With the assistance of metal nanoparticles, molecular hydrogen can be dissociated into active atomic H during the CVD process. Since m-SWCNTs are more chemically

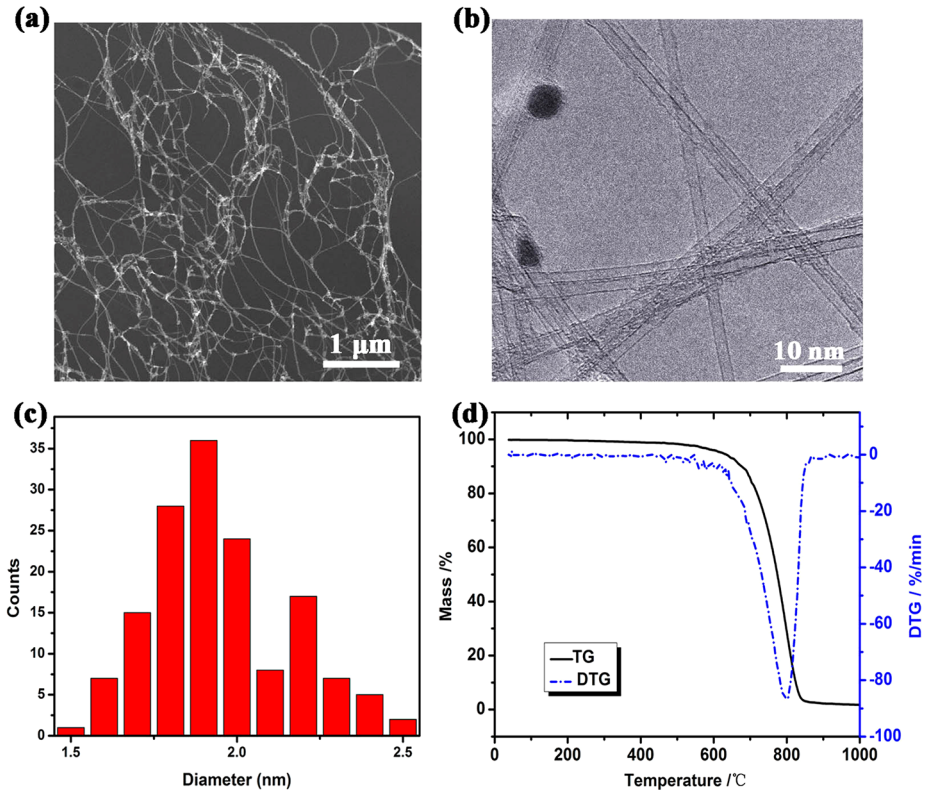

Figure 2. (a) SEM and (b) TEM images of the as-prepared s-SWCNTs. (c) Diameter distribution of the s-SWCNTs. (d) TGA curves of the s-SWCNTs.

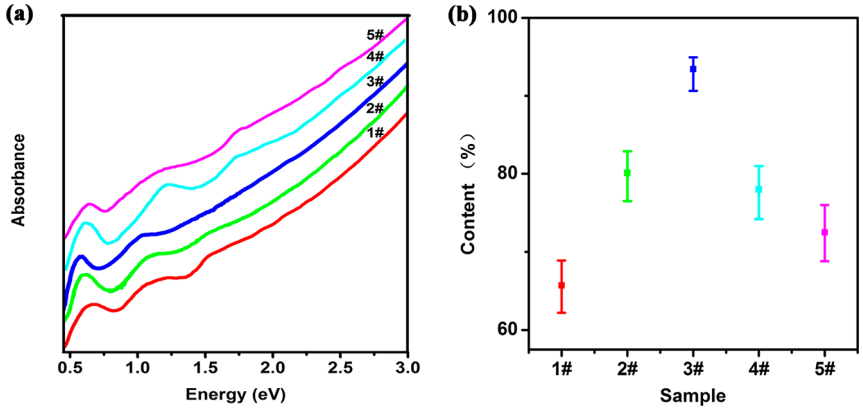

Figure 3. (a) Absorption spectra (0.45−3.0 eV) of samples 1−5#. (b) Contents of s-SWCNTs in these samples estimated from the corresponding absorption peak areas (more detailed calculations are given in S2).

reactive than semiconducting ones due to their smaller ionization potential,[22] and smaller SWCNTs are markedly less stable against hydrocarbonization than larger ones,[17] metallic and small diameter SWCNTs could be preferentially hydrogenated and removed under optimal conditions, which has been confirmed by Raman results. In our FCCVD growth process, sublimated catalyst precursor (ferrocene) is carried into the reaction zone by hydrogen and decomposed into iron nanoparticles. The floating iron catalyst formed *in situ* is highly active and may be more favorable for the dissociation of molecular hydrogen than supported catalysts. As a result, m-SWCNTs with higher reactivity and unstable smaller SWCNTs would be preferentially etched by the atomic H. If we simply assume that the etching rate is determined by the concentration of hydrogen radicals, the amount of atomic H produced using a given temperature and catalyst concentration is obviously related to the flux of hydrogen. Therefore, the content of s-SWCNTs first increases and reaches a maximum value when the hydrogen flow rate is increased to 2000 sccm, but when the hydrogen flow is further increased, the residence time of hydrogen in the high-temperature zone is too short to achieve sufficient dissociation and etching of both m-SWCNTs and small SWCNTs.[36] As a result, an optimum hydrogen

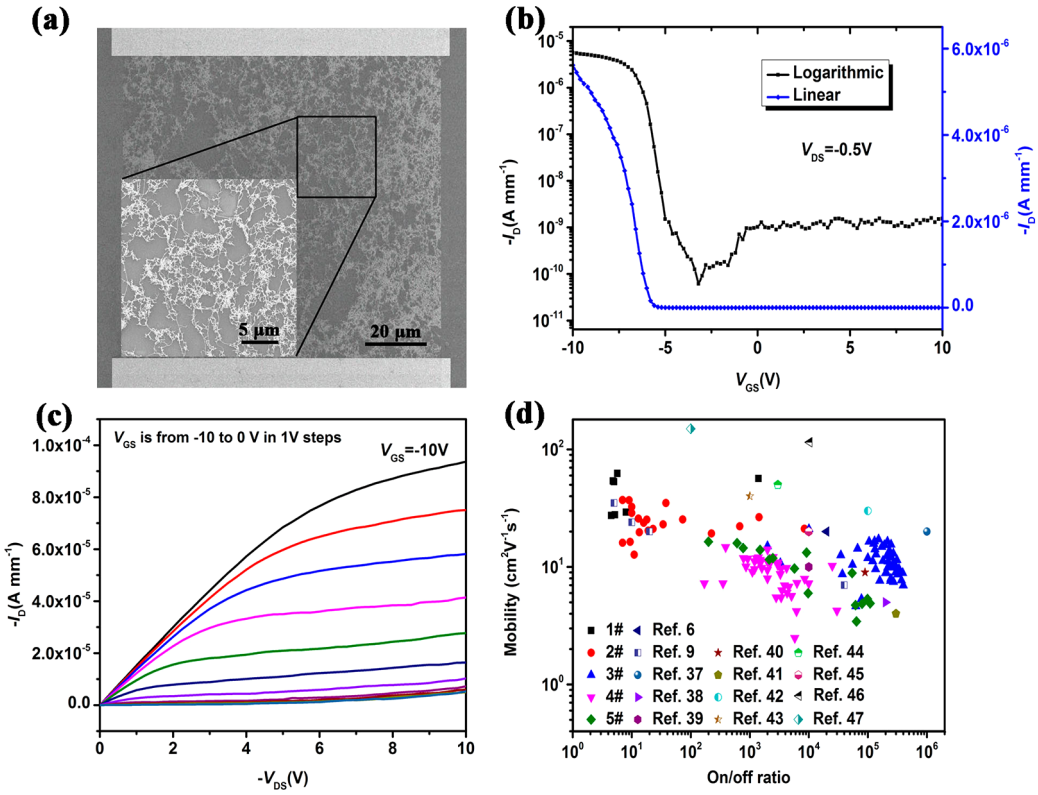

Figure 4. (a) Typical SEM image of the s-SWCNT thin film deposited on a Si substrate. (b) Typical transfer (I_D-V_{GS}) characteristic at V_{DS} of −0.5 V. (c) Output (I_D-V_{DS}) characteristics of the same device at various V_{GS} values ranging from −10 to 0 V. (d) Statistics of the carrier mobilities and on/off ratios of the TFTs fabricated using our 1#, 2#, 3#, 4# and 5# samples in comparison with those reported previously.

flow of 2000 sccm is determined for the selective synthesis of s-SWCNTs.

To verify the effect of hydrogen on the selective synthesis of s-SWCNTs, we performed a comparison experiment using identical parameters except that hydrogen was replaced with helium, which is chemically inert and has a similar thermal conductivity coefficient to that of hydrogen. The synthesis procedure is described in Supporting Information (S1.1). The SWCNTs synthesized with three typical helium flows of 500, 2000, and 4000 sccm were characterized using laser Raman spectroscopy, and the results are shown in Figure S3. RBM peaks originating from both m- and s-SWCNTs are observed for all three samples. Furthermore, the diameter of the SWCNTs synthesized using helium as the carrier gas is obviously smaller than those obtained under a hydrogen flow. Therefore, hydrogen does function as a mild etchant, and the s-SWCNTs were obtained by selective hydrogen etching.

Using the as-prepared s-SWCNT films, we fabricated bottom-gate TFTs on a heavily boron (B)-doped p-Si substrate with a 100 nm thick SiO_2 layer (Figure S1). The channel length (L_{ch}) and channel width (W_{ch}) are both 100 μm (for more details see S1.4). Figure 4a shows a typical SEM image of the SWCNT thin film used. It can be seen that randomly spread SWCNTs form a network on the Si substrate. The gate leakage current associated with the gate bias is on the order of a picoampere and is, therefore, negligible. Figure 4b,c shows the transfer and output characteristics of a typical s-SWCNT TFT. The device showed p-type characteristics with a high on/off ratio of 9.5×10^4 and an effective device carrier mobility of 16.6 cm^2 V^{-1} s^{-1}, which was evaluated by the standard formula:[37]

$$\mu = (L_{ch}/W_{ch})(1/C)(1/V_{DS})(dI_D/dV_{GS})$$

where C is the gate capacitance. We calculated C using a parallel plate model ($C = \varepsilon/\tau_{ox}$), where τ_{ox} and ε are the thickness and dielectric constant of the gate insulator. Figure S4 shows the I_D-V_{GS} curves of 1#, 2#, 3#, 4#, and 5# SWCNT-based TFTs. It can be seen that the 3# SWCNT-based TFTs show high on/off ratios (>10^3) with V_{GS} ranging from 10 to −10 V with a good stability. Figure 4d shows the distributions of carrier mobility and on/off ratio of these five different SWCNT TFTs (for more details, see S1.4), along with a comparison with some previously reported values. As shown, with the increase of hydrogen flow rate, the on/off ratios of the TFTs increase first, and a maximum value is reached with a hydrogen flux of 2000 sccm. The on/off ratio turns begins to decrease with the increase of hydrogen flow. This result is consistent with that from Raman spectra and absorption spectra. On the

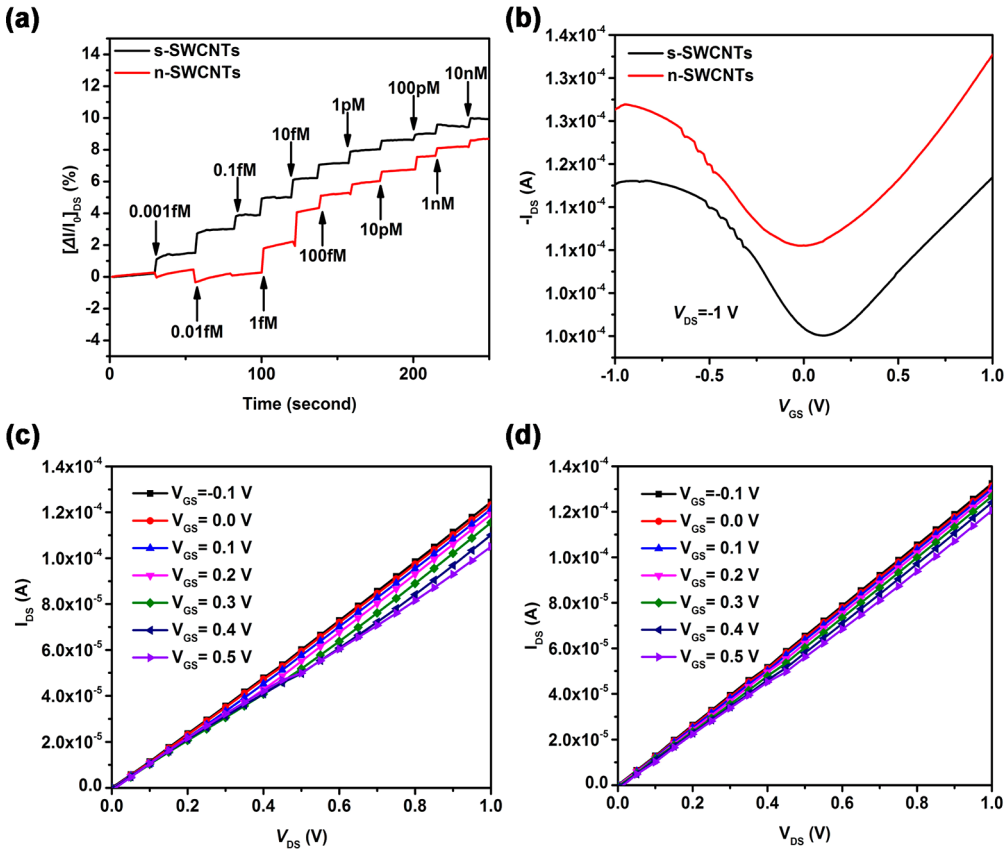

Figure 5. (a) Typical real time current ($\Delta I/I_0$) changes with dopamine concentration in a PBS solution for biosensors based on s- and n-SWCNTs. (b) Typical $I_{DS}-V_{GS}$ curves of the s-SWCNT and n-SWCNT-based biosensors. (c) $I_{DS}-V_{DS}$ curves for the s-SWCNT-based biosensor and (d) n-SWCNT-based biosensor with V_{GS} ranging from −0.1 to 0.5 V using PBS solution as a gate electrode.

contrary, the mobilities of the TFTs decrease at first and reach a low point when the hydrogen flux is 2000 sccm. Then the mobility increases slightly with further increase of hydrogen flow. These results testify that sample 3# has the highest content of s-SWCNTs among the five samples. The maximum carrier mobility achieved is 21.1 $cm^2\ V^{-1}\ s^{-1}$ (with an on/off ratio of 1.1×10^4), and the maximum on/off ratio is 4.0×10^5 (with a carrier mobility of 7.0 $cm^2\ V^{-1}\ s^{-1}$). Compared with the performance of some recently reported FET devices, which were based on SWCNTs,[6,9,37−47] our transistors show a better performance in terms of higher on/off ratio and larger carrier mobility. This can be attributed to the high content of s-SWCNTs with good structural integrity obtained by selective hydrogen etching during growth. Sun *et al.* reported that FETs based on a Y-junction SWCNT network have a high on/off ratio.[37] The SWCNTs they used were not enriched with semiconducting nanotubes, and the high on/off ratio is due to a few interconnected m-SWCNT channels as a result of the very thin film used.

CNTs are an ideal candidate for making sensors because their electronic transport and thermopower (voltages between junctions caused by an interjunction temperature difference) are very sensitive to substances that affect the amount of injected charge.[48,49] We fabricated a biosensor for the detection of dopamine using the synthesized s-SWCNTs. Dopamine is an important catecholamine neurotransmitter existing in the brain and central nervous system of mammals.[50] An abnormal level of dopamine is associated with certain neurological disorders known as schizophrenia, Parkinson's disease, and drug addiction.[51] Therefore, the detection and quantification of dopamine plays a pivotal role in disease diagnosis. Biosensors based on our s-SWCNTs and normal SWCNTs (n-SWCNTs, with no transport property selectivity) were fabricated for comparison (for details, see Figure S5 and S1.5). The current−voltage ($C-V$) characteristics of these sensors were recorded in a solution of 6×10^{-3} mol/L PBS (pH = 7.2) between −1 and 1 V with a scan rate of 10 mV/s and a sample interval of 1 mV. Figure 5a demonstrates the typical real time changes in current ($\Delta I/I_0$) due to the adsorption of dopamine molecules. The s-SWCNT-based device exhibited a very low dopamine detection limit of 10^{-18} mol/L, which is several orders of magnitude lower than the values previously reported.[52−55]

As shown in Figure 5b, the s-SWCNT-based biosensor gives a positive shift (~0.1 mV) in V_{GS}, indicating a typical p-doped (hole-transporting) behavior of s-SWCNTs.[56,57]

The drain-to-source current of the s-SWCNT-based biosensor (I_{DS}, Figure 5c) decreased with an increase of gate V_{GS}, which is characteristic of a liquid ion gate FET,[58] suggesting the obvious p-doped feature of s-SWCNTs, while the I_{DS} of the n-SWCNTs (Figure 5d) showed only a slight decrease under the same increasing V_{GS} rate. The biosensor based on n-SWCNTs has a detection limit 3 orders of magnitude lower than that of the s-SWCNT counterpart, and its V_{GS} and I_{DS} did not change significantly due to the coexistence of m- and s- SWCNTs. It has been reported that the response of CNT-based biosensors to dopamine is likely caused by the aromatic catecholamine molecules of dopamine inducing p-doping (or an increase of hole concentration) in SWCNTs since dopamine can strongly interact with the graphitic layer of SWCNTs through a strong $\pi-\pi$ interaction.[59,60] Based on theoretical calculations,[56,57] the Fermi level of s-SWCNTs shifts close to the valence band due to their easy p-doping feature, which leads to the enrichment of hole carriers in the nanotubes and an increase of sample conductance. For m-SWCNTs, a small shift of the Fermi level does not result in a substantial change in the density of states at the Fermi level and, thus, in charge carriers in the nanotubes. Therefore, the biosensor based on s-SWCNTs is much more sensitive than that based on n-SWCNTs.

CONCLUSIONS

In summary, high-quality, highly concentrated s-SWCNTs were prepared in bulk by *in situ* selective hydrogen etching m-SWCNTs in a floating catalyst CVD growth process. The obtained s-SWCNTs show a very high oxidation resistance temperature of ~800 °C due to their good structural integrity. TFT devices based on the s-SWCNTs demonstrated a high on/off ratio of 4.0×10^5 (with a carrier mobility of 7.0 $cm^2\ V^{-1}\ s^{-1}$) and carrier mobility of 21.1 $cm^2\ V^{-1}\ s^{-1}$ (with an on/off ratio of 1.1×10^4). A biosensor fabricated using the s-SWCNTs showed a very low dopamine detection limit of 10^{-18} mol/L in PBS solution at room temperature. Our work demonstrates a scalable, simple approach to the selective synthesis of high-quality s-SWCNTs that can be potentially used in high-performance transistors, sensors, and other electronic devices.

EXPERIMENTAL SECTION

Synthesis of s-SWCNTs. The SWCNTs were synthesized using a FCCVD method, and the detailed synthesis procedure is described in our previous reports.[12,29] Briefly, ferrocene and sulfur, which respectively serve as the catalyst precursor and growth promoter, were pressed into a tablet and placed at the upstream of a quartz tube reactor in a horizontal tubular furnace. Hydrogen was used as the carrier gas. When the furnace temperature reached 1100 °C, the mixed ferrocene/sulfur tablet (S = 0.5 wt %) was moved to a position with a temperature of ~85 °C, and the sublimated matter was transported into the reaction zone by hydrogen flow. At the same time, 30 sccm CH_4 flow was introduced as a carbon source for SWCNT growth. The products were collected at the downstream of the quartz tube reactor. After a growth time of 30 min, the furnace was cooled naturally to room temperature under the protection of a H_2 flow.

We studied the effect of hydrogen flow rate on the structure and properties of SWCNTs. With CH_4 flow of 30 sccm, catalyst precursor sublimation temperature of 85 °C, and growth temperature of 1100 °C unchanged, we used hydrogen flows of 500, 1000, 2000, 3000, and 4000 sccm (denoted 1#, 2#, 3#, 4#, and 5#, respectively) for the growth of SWCNTs. In order to further confirm the hydrogen etching effect, we also performed comparative experiments using helium as carrier gas instead of hydrogen, and the detailed synthesis process is described in the Supporting Information (S1.1).

Characterization. The morphology, structure, and electrical transport properties of the as-synthesized SWCNTs were characterized using SEM, TEM, multiwavelength laser Raman spectroscopy, absorption spectroscopy, and FET measurements. The detailed sample characterization processes are described in the Supporting Information (S1.6). The oxidation resistance of the sample was evaluated by thermogravimetric (TG) analysis with a thermogravimetric analyzer (NETZSCH STA 449C). It is well-known that Fe catalyst particles can catalyze the oxidation of SWCNTs in oxidizing environments. To reveal the intrinsic oxidation resistance of SWCNTs, the as-synthesized SWCNTs were purified prior to the TG analysis.[29] The detailed purification process is described in the Supporting Information (S1.2).

Biosensors. The as-synthesized s-SWCNTs were directly collected using a rolled aluminum foil at the downstream of the quartz tube reactor, where they were deposited. After a low-temperature oxidation, the SWCNT films were transferred to a polyethylene terephthalate (PET) surface by a stamping method[61] and treated in HCl to remove catalyst particles. The film was cut into small pieces of 1 cm × 2 cm and then connected to a chip carrier using small copper wires at two different points by conductive silver epoxy. More details of the fabrication process of the s-SWCNT films can be found in Supporting Information (S1.5). The operating mechanism of the s-SWCNT sensors presented here is based on changes in their electrical conductivity due to charge transfer induced by the adsorption of molecules acting as donors or acceptors[48,49,60,62,63] on the SWCNT surface. The sensing experiments were performed using trace amounts of dopamine dissolved in PBS at room temperature. Sensors based on both s-SWCNTs and n-SWCNTs were tested for comparison (more details are presented in S3).

Conflict of Interest: The authors declare no competing financial interest.

Acknowledgment. This work was supported by the Ministry of Science and Technology of China (Grants 2011CB932601) and National Natural Science Foundation of China (Grants 51102242, 51221264, 51272256, and 51272257).

Supporting Information Available: Raman spectra, I_D-V_{GS} curves, absorption spectra. This material is available free of charge *via* the Internet at http://pubs.acs.org.

REFERENCES AND NOTES

1. Baughman, R. H.; Zakhidov, A. A.; de Heer, W. A. Carbon Nanotubes—The Route toward Applications. *Science* **2002**, *297*, 787–792.
2. Saito, R.; Dresselhaus, G.; Dresselhaus, M. S. *Physical Properties of Carbon Nanotubes*; Imperial College Press: London, 1998.
3. Komatsu, N.; Wang, F. A Comprehensive Review on Separation Methods and Techniques for Single-Walled Carbon Nanotubes. *Materials* **2010**, *3*, 3818–3844.
4. Tanaka, T.; Jin, H.; Miyata, Y.; Fujii, S.; Suga, H.; Naitoh, Y.; Minari, T.; Miyadera, T.; Tsukagoshi, K.; Kataura, H. Simple

and Scalable Gel-Based Separation of Metallic and Semiconducting Carbon Nanotubes. *Nano Lett.* **2009**, *9*, 1497–1500.
5. Zheng, M.; Jagota, A.; Strano, M. S.; Santos, A. P.; Barone, P.; Chou, S. G.; Diner, B. A.; Dresselhaus, M. S.; Mclean, R. S.; Onoa, G. B. Structure-Based Carbon Nanotube Sorting by Sequence-Dependent DNA Assembly. *Science* **2003**, *302*, 1545–1548.
6. Arnold, M. S.; Green, A. A.; Hulvat, J. F.; Stupp, S. I.; Hersam, M. C. Sorting Carbon Nanotubes by Electronic Structure Using Density Differentiation. *Nat. Nanotechnol.* **2006**, *1*, 60–65.
7. Li, X.; Zhang, L.; Wang, X.; Shimoyama, I.; Sun, X.; Seo, W. S.; Dai, H. Langmuir−Blodgett Assembly of Densely Aligned Single-Walled Carbon Nanotubes from Bulk Materials. *J. Am. Chem. Soc.* **2007**, *129*, 4890–4891.
8. Voggu, R.; Rao, K. V.; George, S. J.; Rao, C. A Simple Method of Separating Metallic and Semiconducting Single-Walled Carbon Nanotubes Based on Molecular Charge Transfer. *J. Am. Chem. Soc.* **2010**, *132*, 5560–5561.
9. Behnam, A.; Sangwan, V. K.; Zhong, X.; Lian, F.; Estrada, D.; Jariwala, D.; Hoag, A. J.; Lauhon, L. J.; Marks, T. J.; Hersam, M. C. High-Field Transport and Thermal Reliability of Sorted Carbon Nanotube Network Devices. *ACS Nano* **2012**, *7*, 482–490.
10. Tulevski, G. S.; Franklin, A. D.; Afzali, A. High Purity Isolation and Quantification of Semiconducting Carbon Nanotubes *via* Column Chromatography. *ACS Nano* **2013**, *7*, 2971–2976.
11. Qi, H.; Qian, C.; Liu, J. Synthesis of High-Purity Few-Walled Carbon Nanotubes from Ethanol/Methanol Mixture. *Chem. Mater.* **2006**, *18*, 5691–5695.
12. Yu, B.; Liu, C.; Hou, P. X.; Tian, Y.; Li, S.; Liu, B.; Li, F.; Kauppinen, E. I.; Cheng, H. M. Bulk Synthesis of Large Diameter Semiconducting Single-Walled Carbon Nanotubes by Oxygen-Assisted Floating Catalyst Chemical Vapor Deposition. *J. Am. Chem. Soc.* **2011**, *133*, 5232–5235.
13. Zhou, W.; Zhan, S.; Ding, L.; Liu, J. General Rules for Selective Growth of Enriched Semiconducting Single Walled Carbon Nanotubes with Water Vapor as *In-Situ* Etchant. *J. Am. Chem. Soc.* **2012**, *134*, 14019–14026.
14. Li, S.; Liu, C.; Hou, P. X.; Sun, D. M.; Cheng, H. M. Enrichment of Semiconducting Single-Walled Carbon Nanotubes by Carbothermic Reaction for Use in All-Nanotube Field Effect Transistors. *ACS Nano* **2012**, *6*, 9657–9661.
15. Hassanien, A.; Tokumoto, M.; Umek, P.; Vrbanič, D.; Mozetič, M.; Mihailović, D.; Venturini, P.; Pejovnik, S. Selective Etching of Metallic Single-Wall Carbon Nanotubes with Hydrogen Plasma. *Nanotechnology* **2005**, *16*, 278.
16. Zhang, G.; Qi, P.; Wang, X.; Lu, Y.; Li, X.; Tu, R.; Bangsaruntip, S.; Mann, D.; Zhang, L.; Dai, H. Selective Etching of Metallic Carbon Nanotubes by Gas-Phase Reaction. *Science* **2006**, *314*, 974–977.
17. Zhang, G.; Qi, P.; Wang, X.; Lu, Y.; Mann, D.; Li, X.; Dai, H. Hydrogenation and Hydrocarbonation and Etching of Single-Walled Carbon Nanotubes. *J. Am. Chem. Soc.* **2006**, *128*, 6026–6027.
18. Liu, C.; Cheng, H. M.; Cong, H.; Li, F.; Su, G.; Zhou, B.; Dresselhaus, M. Synthesis of Macroscopically Long Ropes of Well-Aligned Single-Walled Carbon Nanotubes. *Adv. Mater.* **2000**, *12*, 1190–1192.
19. Liu, C.; Cong, H.; Li, F.; Tan, P.; Cheng, H.; Lu, K.; Zhou, B. Semi-Continuous Synthesis of Single-Walled Carbon Nanotubes by a Hydrogen Arc Discharge Method. *Carbon* **1999**, *37*, 1865–1868.
20. Talyzin, A. V.; Luzan, S.; Anoshkin, I. V.; Nasibulin, A. G.; Jiang, H.; Kauppinen, E. I.; Mikoushkin, V. M.; Shnitov, V. V.; Marchenko, D. E.; Noréus, D. Hydrogenation, Purification, and Unzipping of Carbon Nanotubes by Reaction with Molecular Hydrogen: Road to Graphane Nanoribbons. *ACS Nano* **2011**, *5*, 5132–5140.
21. Yu, F.; Zhou, H.; Yang, H.; Chen, M.; Wang, G.; Sun, L. Preferential Elimination of Thin Single-Walled Carbon Nanotubes by Iron Etching. *Chem. Commun.* **2012**, *48*, 1042–1044.
22. Ding, L.; Tselev, A.; Wang, J.; Yuan, D.; Chu, H.; McNicholas, T. P.; Li, Y.; Liu, J. Selective Growth of Well-Aligned Semiconducting Single-Walled Carbon Nanotubes. *Nano Lett.* **2009**, *9*, 800–805.
23. Luo, Z.; Pfefferle, L. D.; Haller, G. L.; Papadimitrakopoulos, F. (*n*,*m*) Abundance Evaluation of Single-Walled Carbon Nanotubes by Fluorescence and Absorption Spectroscopy. *J. Am. Chem. Soc.* **2006**, *128*, 15511–15516.
24. Strano, M. S. Probing Chiral Selective Reactions Using a Revised Kataura Plot for the Interpretation of Single-Walled Carbon Nanotube Spectroscopy. *J. Am. Chem. Soc.* **2003**, *125*, 16148–16153.
25. Strano, M. S.; Dyke, C. A.; Usrey, M. L.; Barone, P. W.; Allen, M. J.; Shan, H.; Kittrell, C.; Hauge, R. H.; Tour, J. M.; Smalley, R. E. Electronic Structure Control of Single-Walled Carbon Nanotube Functionalization. *Science* **2003**, *301*, 1519–1522.
26. Jorio, A.; Souza Filho, A.; Dresselhaus, G.; Dresselhaus, M.; Swan, A.; Unlü, M.; Goldberg, B.; Pimenta, M.; Hafner, J.; Lieber, C. G-Band Resonant Raman Study of 62 Isolated Single-Wall Carbon Nanotubes. *Phys. Rev. B* **2002**, *65*, 155412.
27. Uchida, T.; Tachibana, M.; Kurita, S.; Kojima, K. Temperature Dependence of the Breit-Wigner-Fano Raman Line in Single-Wall Carbon Nanotube Bundles. *Chem. Phys. Lett.* **2004**, *400*, 341–346.
28. Jorio, A.; Pimenta, M.; Souza Filho, A.; Saito, R.; Dresselhaus, G.; Dresselhaus, M. Characterizing Carbon Nanotube Samples with Resonance Raman Scattering. *New J. Phys.* **2003**, *5*, 139.
29. Yu, B.; Hou, P. X.; Li, F.; Liu, B.; Liu, C.; Cheng, H. M. Selective Removal of Metallic Single-Walled Carbon Nanotubes by Combined *In Situ* and Post-synthesis Oxidation. *Carbon* **2010**, *48*, 2941–2947.
30. Huang, H.; Kajiura, H.; Tsutsui, S.; Murakami, Y.; Ata, M. High-Quality Double-Walled Carbon Nanotube Super Bundles Grown in a Hydrogen-Free Atmosphere. *J. Phys. Chem. B* **2003**, *107*, 8794–8798.
31. Zhang, H.; Sun, C. H.; Li, F.; Li, H. X.; Cheng, H. M. Purification of Multiwalled Carbon Nanotubes by Annealing and Extraction Based on the Difference in van der Waals Potential. *J. Phys. Chem. B* **2006**, *110*, 9477–9481.
32. Nair, N.; Usrey, M. L.; Kim, W. J.; Braatz, R. D.; Strano, M. S. Estimation of the (*n*,*m*) Concentration Distribution of Single-Walled Carbon Nanotubes from Photoabsorption Spectra. *Anal. Chem.* **2006**, *78*, 7689–7696.
33. Ryabenko, A.; Dorofeeva, T.; Zvereva, G. UV−Vis−NIR Spectroscopy Study of Sensitivity of Single-Wall Carbon Nanotubes to Chemical Processing and van-der-Waals SWNT/SWNT Interaction. Verification of the SWNT Content Measurements by Absorption Spectroscopy. *Carbon* **2004**, *42*, 1523–1535.
34. Tian, Y.; Jiang, H.; von Pfaler, J.; Zhu, Z.; Nasibulin, A. G.; Nikitin, T.; Aitchison, B.; Khriachtchev, L.; Brown, D. P.; Kauppinen, E. I. Analysis of the Size Distribution of Single-Walled Carbon Nanotubes Using Optical Absorption Spectroscopy. *J. Phys. Chem. Lett.* **2010**, *1*, 1143–1148.
35. Miyata, Y.; Yanagi, K.; Maniwa, Y.; Kataura, H. Optical Evaluation of the Metal-to-Semiconductor Ratio of Single-Wall Carbon Nanotubes. *J. Phys. Chem. C* **2008**, *112*, 13187–13191.
36. Conroy, D.; Moisala, A.; Cardoso, S.; Windle, A.; Davidson, J. Carbon Nanotube Reactor: Ferrocene Decomposition, Iron Particle Growth, Nanotube Aggregation and Scale-Up. *Chem. Eng. Sci.* **2010**, *65*, 2965–2977.
37. Sun, D.; Timmermans, M. Y.; Tian, Y.; Nasibulin, A. G.; Kauppinen, E. I.; Kishimoto, S.; Mizutani, T.; Ohno, Y. Flexible High-Performance Carbon Nanotube Integrated Circuits. *Nat. Nanotechnol.* **2011**, *6*, 156–161.
38. LeMieux, M. C.; Roberts, M.; Barman, S.; Jin, Y. W.; Kim, J. M.; Bao, Z. Self-Sorted, Aligned Nanotube Networks for Thin-Film Transistors. *Science* **2008**, *321*, 101–104.
39. Engel, M.; Small, J. P.; Steiner, M.; Freitag, M.; Green, A. A.; Hersam, M. C.; Avouris, P. Thin Film Nanotube Transistors Based on Self-Assembled, Aligned, Semiconducting Carbon Nanotube Arrays. *ACS Nano* **2008**, *2*, 2445–2452.

40. Snow, E.; Novak, J.; Campbell, P.; Park, D. Random Networks of Carbon Nanotubes as an Electronic Material. *Appl. Phys. Lett.* **2003**, *82*, 2145–2147.
41. Zavodchikova, M. Y.; Kulmala, T.; Nasibulin, A. G.; Ermolov, V.; Franssila, S.; Grigoras, K.; Kauppinen, E. I. Carbon Nanotube Thin Film Transistors Based on Aerosol Methods. *Nanotechnology* **2009**, *20*, 085201.
42. Cao, Q.; Kim, H. S.; Pimparkar, N.; Kulkarni, J. P.; Wang, C.; Shim, M.; Roy, K.; Alam, M. A.; Rogers, J. A. Medium-Scale Carbon Nanotube Thin-Film Integrated Circuits on Flexible Plastic Substrates. *Nature* **2008**, *454*, 495–500.
43. Cao, Q.; Xia, M. G.; Shim, M.; Rogers, J. A. Bilayer Organic–Inorganic Gate Dielectrics for High-Performance, Low-Voltage, Single-Walled Carbon Nanotube Thin-Film Transistors, Complementary Logic Gates, and p-n Diodes on Plastic Substrates. *Adv. Funct. Mater.* **2006**, *16*, 2355–2362.
44. Ha, M.; Xia, Y.; Green, A. A.; Zhang, W.; Renn, M. J.; Kim, C. H.; Hersam, M. C.; Frisbie, C. D. Printed, Sub-3V Digital Circuits on Plastic from Aqueous Carbon Nanotube Inks. *ACS Nano* **2010**, *4*, 4388–4395.
45. Wang, C.; Zhang, J.; Ryu, K.; Badmaev, A.; De Arco, L. G.; Zhou, C. Wafer-Scale Fabrication of Separated Carbon Nanotube Thin-Film Transistors for Display Applications. *Nano Lett.* **2009**, *9*, 4285–4291.
46. Che, Y.; Wang, C.; Liu, J.; Liu, B.; Lin, X.; Parker, J.; Beasley, C.; Wong, H.-S. P.; Zhou, C. Selective Synthesis and Device Applications of Semiconducting Single-Walled Carbon Nanotubes Using Isopropyl Alcohol as Feedstock. *ACS Nano* **2012**, *6*, 7454–7462.
47. Snow, E.; Campbell, P.; Ancona, M.; Novak, J. High-Mobility Carbon-Nanotube Thin-Film Transistors on a Polymeric Substrate. *Appl. Phys. Lett.* **2005**, *86*, 033105.
48. Collins, P. G.; Bradley, K.; Ishigami, M.; Zettl, A. Extreme Oxygen Sensitivity of Electronic Properties of Carbon Nanotubes. *Science* **2000**, *287*, 1801–1804.
49. Kong, J.; Franklin, N. R.; Zhou, C.; Chapline, M. G.; Peng, S.; Cho, K.; Dai, H. Nanotube Molecular Wires as Chemical Sensors. *Science* **2000**, *287*, 622–625.
50. Venton, B. J.; Wightman, R. M. Psychoanalytical Electrochemistry: Dopamine and Behavior. *Anal. Chem.* **2003**, *75*, 414–421.
51. Baldrich, E.; Gómez, R.; Gabriel, G.; Muñoz, F. X. Magnetic Entrapment for Fast, Simple and Reversible Electrode Modification with Carbon Nanotubes: Application to Dopamine Detection. *Biosens. Bioelectron.* **2011**, *26*, 1876–1882.
52. Ali, S. R.; Ma, Y.; Parajuli, R. R.; Balogun, Y.; Lai, W. Y. C.; He, H. A Nonoxidative Sensor Based on a Self-Doped Polyaniline/Carbon Nanotube Composite for Sensitive and Selective Detection of the Neurotransmitter Dopamine. *Anal. Chem.* **2007**, *79*, 2583–2587.
53. Britto, P.; Santhanam, K.; Ajayan, P. Carbon Nanotube Electrode for Oxidation of Dopamine. *Bioelectrochem. Bioenerg.* **1996**, *41*, 121–125.
54. Fabre, B.; Taillebois, L. Poly(aniline boronic acid)-Based Conductimetric Sensor of Dopamine. *Chem. Commun.* **2003**, 2982–2983.
55. Zhang, P.; Wu, F. H.; Zhao, G. C.; Wei, X. W. Selective Response of Dopamine in the Presence of Ascorbic Acid at Multi-Walled Carbon Nanotube Modified Gold Electrode. *Bioelectrochemistry* **2005**, *67*, 109–114.
56. Grujicic, M.; Cao, G.; Singh, R. The Effect of Topological Defects and Oxygen Adsorption on the Electronic Transport Properties of Single-Walled Carbon-Nanotubes. *Appl. Surf. Sci.* **2003**, *211*, 166–183.
57. Jhi, S. H.; Louie, S. G.; Cohen, M. L. Electronic Properties of Oxidized Carbon Nanotubes. *Phys. Rev. Lett.* **2000**, *85*, 1710–1713.
58. Park, S. J.; Kwon, O. S.; Lee, S. H.; Song, H. S.; Park, T. H.; Jang, J. Ultrasensitive Flexible Graphene Based FET-Type Bioelectronic Nose. *Nano Lett.* **2012**, *12*, 5082–5090.
59. Dong, X.; Fu, D.; Fang, W.; Shi, Y.; Chen, P.; Li, L. J. Doping Single-Layer Graphene with Aromatic Molecules. *Small* **2009**, *5*, 1422–1426.
60. He, Q.; Sudibya, H. G.; Yin, Z.; Wu, S.; Li, H.; Boey, F.; Huang, W.; Chen, P.; Zhang, H. Centimeter-Long and Large-Scale Micropatterns of Reduced Graphene Oxide Films: Fabrication and Sensing Applications. *ACS Nano* **2010**, *4*, 3201–3208.
61. Kaskela, A.; Nasibulin, A. G.; Timmermans, M. Y.; Aitchison, B.; Papadimitratos, A.; Tian, Y.; Zhu, Z.; Jiang, H.; Brown, D. P.; Zakhidov, A. Aerosol-Synthesized SWCNT Networks with Tunable Conductivity and Transparency by a Dry Transfer Technique. *Nano Lett.* **2010**, *10*, 4349–4355.
62. Star, A.; Joshi, V.; Skarupo, S.; Thomas, D.; Gabriel, J. C. P. Gas Sensor Array Based on Metal-Decorated Carbon Nanotubes. *J. Phys. Chem. B* **2006**, *110*, 21014–21020.
63. Sudibya, H. G.; He, Q.; Zhang, H.; Chen, P. Electrical Detection of Metal Ions Using Field-Effect Transistors Based on Micropatterned Reduced Graphene Oxide Films. *ACS Nano* **2011**, *5*, 1990–1994.